JOURNAL OF MATERIALS SCIENCE: MATERIALS IN MEDICINE 10 (1999) 269–273

Preparation and characterization of bioactive monolayer and functionally graded coatings

M. WANG, X. Y. YANG, K. A. KHOR, Y. WANG
School of Mechanical and Production Engineering, Nanyang Technological University, Nanyang Avenue, Singapore 639798

Hydroxyapatite powders were made by reacting orthophosphoric acid with calcium hydroxide and dense bioactive coatings were subsequently produced by the plasma spray technique. Three types of hydroxyapatite (flame spheroidized) monolayer coatings and three types of functionally graded coatings were manufactured. It was found that average microhardness values of monolayer coatings decreased as the indentation load increased. The relationship between indentation load and indent diagonal length observed Meyer's law. Microhardness and fracture toughness of coatings were affected by characteristics of feedstock powders for plasma spraying. The indentation fracture toughness of coatings could be significantly increased by incorporating a toughening phase.

1. Introduction

Hydroxyapatite (HA) has been used in various forms in the medical field due to its similarity to bone apatite. Being osteoconductive, one of its applications is to form a coating on metallic implants to serve as an interfacial bioactive phase between the implant and surrounding tissue after implantation [1–4]. In addition to bioactivity, a satisfactory HA coating must be dense, hard, adherent and tough for clinical uses. However, HA is a brittle and relatively weak ceramic. Therefore, some tough but bioinert ceramics such as TiO_2, Al_2O_3 and ZrO_2 were used to form bioactive ceramic composites for improved mechanical performances [5–7]. Other calcium phosphates such as tricalcium phosphate (α-TCP) can also be considered for toughening HA [8]. Additionally, due to its resorbability, TCP in the HA-based composites can gradually dissolve after implantation so as to promote enhanced osseointegration [9].

One method to improve properties of coatings and the bonding strength between the coating and the substrate is to employ a coating with a novel structure. A functionally graded material, which has a compositional gradient from the surface to the interior of the material, can be used for such purposes. To strike a balance between mechanical properties and biocompatibility, a three-layer functionally graded coating (FGC) structure was designed [10]. The sub-layer which bonds with the substrates should be a mechanical support for the whole coating system. In the mean time, the sub-layer on the surface of the FGC should be bioactive (or bioresorbable) in order to obtain excellent biocompatibility with osseous tissues. The sub-layer which is located between the aforementioned layers may have a compromised mechanical/biological performance.

In the current investigation, monolayer HA coatings and bioactive FGCs were produced by the plasma spray technique according to the adhesive strength and bioactivity (or bioresorbability) of various components in the coatings. This paper presents some preliminary results on microstructure and mechanical properties of these coatings.

2. Materials and methods

HA powders for plasma spraying were produced using the precipitation method [11, 12]. Two solutions, orthophosphoric acid (H_3PO_4) and calcium hydroxide ($Ca(OH)_2$) with a concentration of 1 M, were used for the reaction

$$10Ca(OH)_2 + 6H_3PO_4 \longrightarrow Ca_{10}(PO_4)_6(OH)_2 + 18H_2O \quad (1)$$

The reaction temperature was carefully controlled at 40 °C. The precipitated HA powder was spray dried at 200 °C. The spray dried powder was then spheroidized by combustion flame spraying it into distilled water. It was finally oven dried for plasma spraying. A vibratory sieving system was used to separate the flame sprayed HA powders into three particle size ranges (R_p): 20 ~ 45 μm, 45 ~ 75 μm and 75 ~ 125 μm.

The flame spheroidized HA (SHA) powders were sprayed onto Ti–6Al–4V plates to form bioactive coatings by using a 40 kW plasma spray system (SG-100, Miller Thermal Inc., Wisconsin, USA). Argon was used as the main plasma forming gas and helium the auxiliary gas with a pressure of 0.28 MPa for each gas. The feed rate of powders was about 20 g min^{-1} and the

Corresponding author: Dr Min Wang

spraying distance was $8 \sim 10$ cm. The current and voltage of the plasma spraying arc were 800 A and 30 V, respectively. Three types of FGCs were obtained by using (a) SHA powders with different R_p, (b) mixtures of SHA and spherical α-TCP powders, and (c) mixtures of SHA and TiO_2 powders (Table I). The thickness was around 400 μm for each monolayer SHA coating and approximately 130 μm for each sub-layer in FGCs.

Phases of powders and bioactive coatings were analyzed by using a Philips MPD 1880 X-ray diffractometer (XRD), while chemical components were detected by using energy dispersive X-ray spectroscopy (EDX). Cross-sections of coatings were prepared following an established procedure [12]. Microhardness tests were then performed on these cross-sections using Shimadzu HMV-2000 and HSV-20 hardness testers. Pyramid-shaped diamond indenters were used and Vicker's hardness values (VHN) obtained. Indentation loads were 0.1, 0.2, 1.0, 2.0 and 2.5 kgf and the holding time remained 15 s for all tests. At least five indents were made for each monolayer SHA coating and every sub-layer of FGCs. In the case of investigating hardness variations across the thickness of coatings, an indentation load of 0.1 kgf was used so as to obtain small indents. A repeat run was conducted to verify the trend of hardness changes. A Cambridge Stereoscan 360 scanning electron microscope (SEM) was used to examine the powder morphology, the microstructure of bioactive coatings and the shape of Vicker's indents. If indentation cracks had been induced, the crack lengths were also measured under SEM for the calculation of fracture toughness of various coatings.

3. Results and discussion

An EDX spectrum of spray dried HA powder is shown in Fig. 1. It can be seen that the main elements of the powder were calcium and phosphorus. The molar ratio of calcium to phosphorus was approximately 10 : 6, which is the stoichiometric value for pure hydroxyapatite. Fig. 2 shows morphologies of spray dried and flame spheroidized HA powders. The mean particle size of spray-dried HA powder was within 50 μm and the particle size distribution was narrower than the $Ca(OH)_2$ powder used for the reaction. Some pores could be found on the surface of spray-dried particles, indicating that the density of these particles was lower than that of bulk HA. After flame spheroidization, the shape of HA particles became spherical and the mean particle size decreased. XRD patterns of spray-dried and flame spheroidized powders are shown in Fig. 3. Comparing these patterns with the standard pattern for HA, it is demonstrated that the powders were composed of pure HA and the amorphous phase. Because the peak/background ratio was low while the width of peaks was wide, the amount of amorphous phase in the spray-dried powders was thought to be high. It was noted that the relative crystallinity of HA increased and that no decomposition of HA was encountered through flame spheroidization.

It was found that SHA significantly improved processability during plasma spraying and hence good

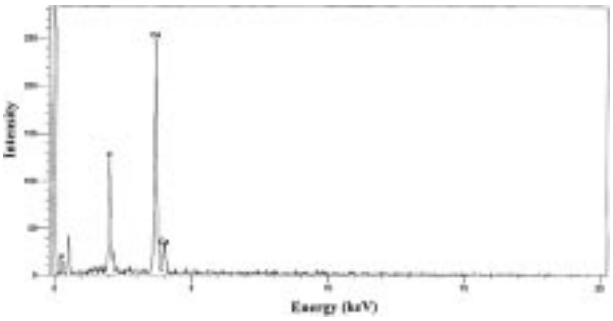

Figure 1 An EDX spectrum of spray dried hydroxyapatite powder.

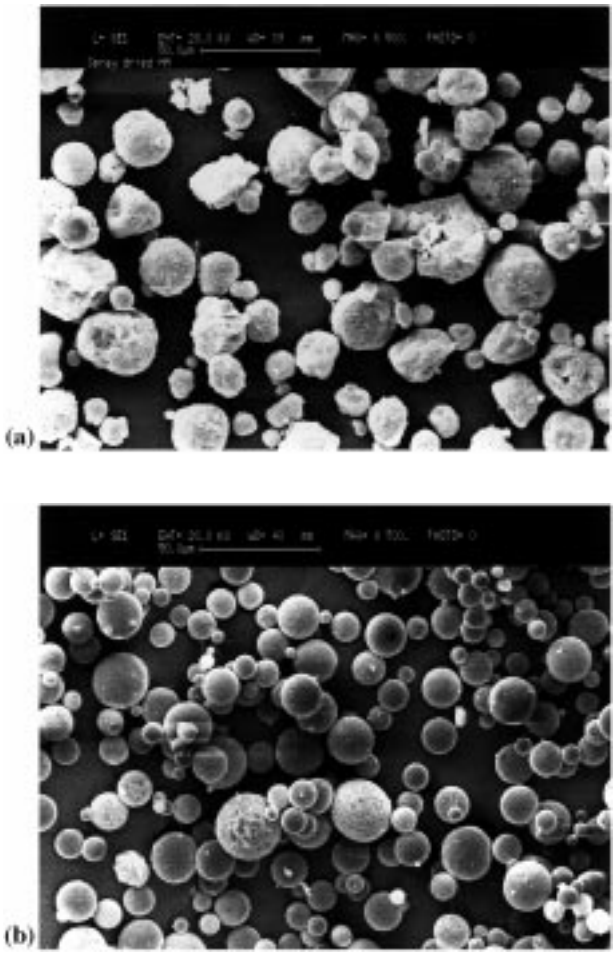

Figure 2 Morphology of hydroxyapatite powder: (a) spray-dried; (b) flame spheroidized.

TABLE I Composition of functionally graded coatings

Designation	First layer*	Second layer	Third layer
FGC1	SHA (R_p: 20 ~ 45 μm)	SHA (R_p: 45 ~ 75 μm)	SHA (R_p: 75 ~ 125 μm)
FGC2	SHA (R_p: 20 ~ 45 μm)	50 wt % SHA, 50 wt % α-TCP	α-TCP
FGC3	TiO_2	50 wt % TiO_2, 50 wt % SHA	SHA (R_p: 75 ~ 125 μm)

*The first layer refers to the layer next to the Ti–6Al–4V substrate.

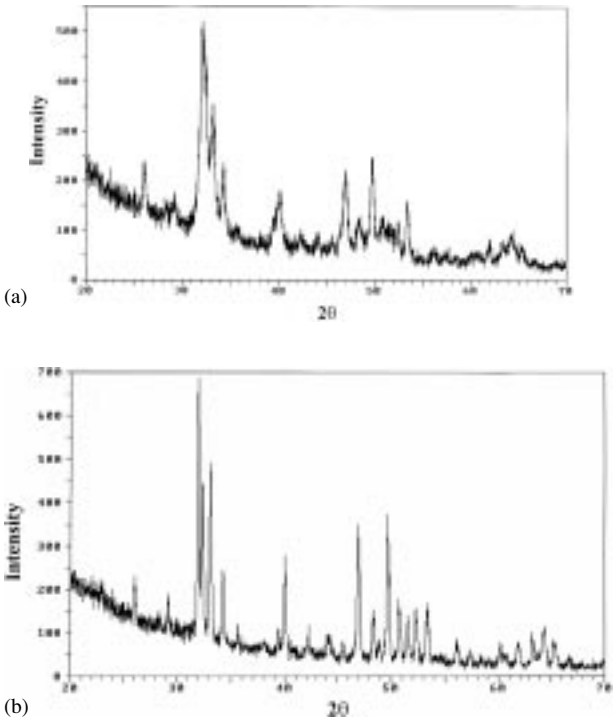

Figure 3 XRD pattern of hydroxyapatite powder: (a) spray-dried; (b) flame spheroidized.

quality monolayer coatings and FGCs could be routinely produced. Fig. 4 is an SEM micrograph of the cross-section of an as-sprayed SHA coating. The as-sprayed coatings were dense and the microstructure was composed of several randomly stacked lamellae. Some micropores and microcracks could be seen at the intersections of these lamellae. The cracks induced by micro-indentation may therefore propagate along the inter-lamellae defects. XRD patterns of plasma-sprayed SHA coatings (Fig. 5) showed that, apart from HA, the coatings also contained some other phases such as α-TCP, CaO and tetracalcium phosphate (TTCP). The appearance of these new phases was due to the decomposition of HA caused by the high temperature within the plasma flame. Peak heights of the HA phase decreased and its width became broad due to the formation of the amorphous phase during the plasma spray process.

Fig. 6 exhibits a Vicker's indent in an SHA coating. It was found that indentation cracks could not be produced in SHA coatings when the indentation load was below 1.0 kgf, but the four edges of Vickers indents were distinct under such loads. When the indentation load was above 1.0 kgf, the length of induced microcracks became longer as the indentation load increased. The initiation site of microcracks induced was not the exact tip of the indent diagonal but near inter-lamellae defects. The propagation of induced microcracks parallel to HA lamellae demonstrated anisotropy of the coatings produced by plasma spraying. Such phenomena were observed in all three types of monolayer SHA coatings.

The microhardness test results of SHA coatings are tabulated in Table II. It was evident that microhardness of as-sprayed SHA coatings was affected by characteristics of feedstock powders. With a relatively small particle size, a much denser HA coating could be obtained and

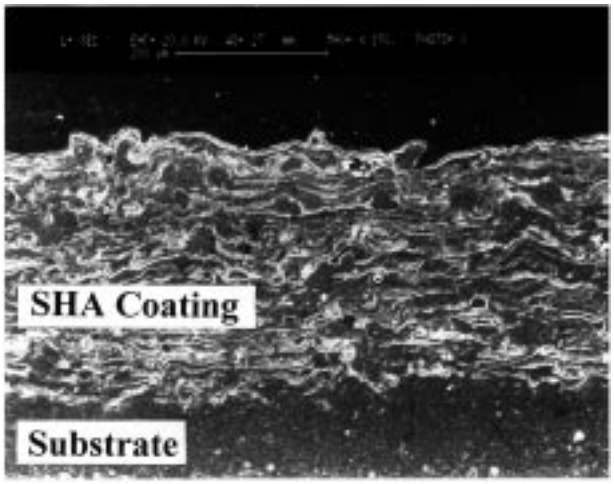

Figure 4 A cross-section of monolayer SHA coating.

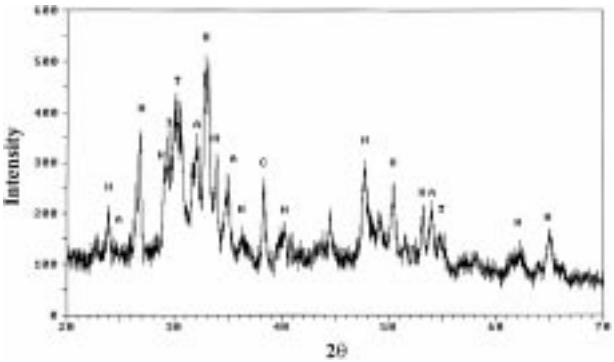

Figure 5 XRD pattern of a plasma-sprayed SHA coating; A:α-TCP; C:CaO, H:HA, T:TTCP.

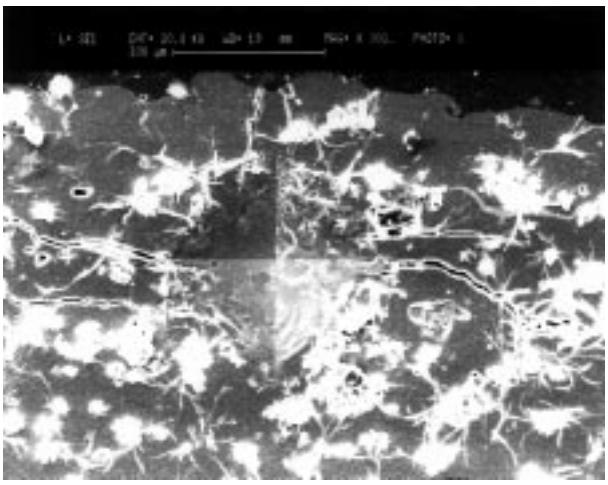

Figure 6 A Vicker's indent and induced microcracks in an SHA coating (R_p: 45 ~ 75 μm).

mechanical properties of the coating would be consequently better. The microhardness value decreased with an increase in indentation load. It was found that indentation load (L) and indent diagonal length (d) observed Meyer's law [13] for SHA coatings

$$L = a \times d^n \qquad (2)$$

where a is a material-related constant and n the Meyer parameter. Fig. 7 shows Meyer's plots for monolayer

TABLE II Microhardness of monolayer SHA coatings

Indentation load	Microhardness (VHN)*		
(kgf)	R_p: 20 ~ 45 μm	R_p: 45 ~ 75 μm	R_p: 75 ~ 125 μm
0.1	330 ± 20	302 ± 18	270 ± 15
0.2	291 ± 17	274 ± 15	242 ± 14
1.0	267 ± 15	251 ± 14	221 ± 14
2.0	256 ± 14	234 ± 13	209 ± 13
2.5	247 ± 14	228 ± 12	199 ± 12

*mean ± SD.

SHA coatings. The Meyer parameter n was 1.84, 1.85 and 1.85 for coatings with R_p in the range of 20 ~ 45 μm, 45 ~ 75 μm and 75 ~ 125 μm, respectively. Microhardness (H) is expressed by the following equation

$$H = A \times L \times d^{-2} \quad (3)$$

where A is a constant. Therefore, H and L can be correlated as

$$H = B \times L^{1-(2/n)} \quad (4)$$

where B is a constant. Because n is lower than 2 in the case of SHA coatings, the microhardness value decreases as the indentation load increases. Results obtained from other ceramic materials show a similar trend [14].

Fig. 8 depicts the variation of microhardness in FGC 1. The sub-layer with a large particle size possessed low microhardness and the average microhardness value of each sub-layer was similar to the monolayer SHA coating with the same R_p. Results obtained from microhardness tests demonstrated that properties of plasma sprayed coatings could be affected significantly by characteristics of feedstock powders. Fig. 9 shows the variation of microhardness in FGC 3. The first sub-layer which was composed of TiO_2 exhibited a high microhardness value (around 940 VHN). Microhardness decreased dramatically to about 400 VHN in the second layer which had 50 wt % of SHA. The microhardness value of the third layer (i.e. the SHA layer) was comparable to the value obtained for the monolayer SHA coating as shown in Table II. It was noticed that microhardness in the transitional area between adjacent layers was relatively low. These low values may be attributed to the relatively high (tensile) residential stress at these locations. The repeat tests verified these trends.

The indentation fracture toughness (K_{IC}) can be calculated using the following equation [15]

$$K_{IC} = 0.016(E/H)^{1/2}(L/C^{3/2}) \quad (5)$$

where E is Young's modulus of the coating and C the crack length. Assuming Young's modulus of HA was 100 GPa [16], fracture toughness values of SHA coatings and sub-layers of FGC 1 were obtained (Table III). It was noted that K_{IC} decreased as the feedstock particle size increased. K_{IC} was around 1 MPa m$^{-1/2}$ when the particle size was below 45 μm. It decreased to less than 0.6 MPa m$^{-1/2}$ when the particle size was above 45 μm. Results for the three sub-layers of FGC 1 were similar to those of respective monolayer SHA coatings with the same R_p. The fracture toughness of SHA coatings

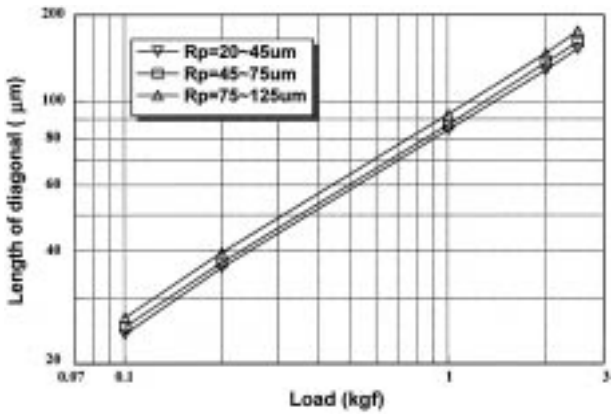

Figure 7 Meyer's plots for monolayer SHA coatings.

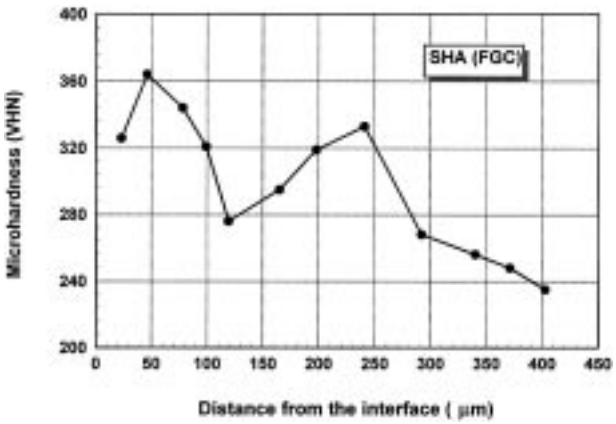

Figure 8 Variation of microhardness in FGC 1.

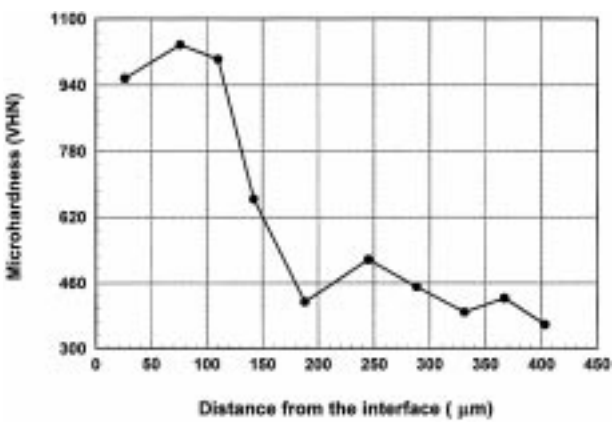

Figure 9 Variation of microhardness in FGC 3.

TABLE III Fracture toughness of monolayer SHA coatings and sub-layers of FGC 1

Designation of coatings	SHA (R_p: 20 ~ 45 μm)	SHA (R_p: 45 ~ 75 μm)	SHA (R_p: 75 ~ 125 μm)	FGC1 (1st layer)	FGC1 (2nd layer)	FGC1 (3rd layer)
K_{IC} (MPa m$^{-1/2}$)*	0.95 ± 0.02	0.55 ± 0.01	0.46 ± 0.01	1.05 ± 0.03	0.57 ± 0.01	0.47 ± 0.01

*mean ± SD.

TABLE IV Fracture toughness of sub-layers of FGC 2 and FGC 3

Designation of coatings	FGC2 (1st layer)	FGC2 (2nd layer)	FGC2 (3rd layer)	FGC3 (1st layer)	FGC3 (2nd layer)	FGC3 (3rd layer)
K_{IC} (MPa m$^{-1/2}$)*	1.05 ± 0.02	1.28 ± 0.02	1.41 ± 0.03	–†	1.76 ± 0.03	0.47 ± 0.01

*mean ± SD.
†Microcracks could not be induced under the indentation load of 2.0 kgf.

obtained in this study was in broad agreement with other investigations [8]. Fracture toughness of each sub-layer of FGC 2 and FGC 3 is shown in Table IV. K_{IC} of α-TCP in FGC 2 was about 1.41 MPa m$^{-1/2}$, which is higher than that of SHA coatings. Furthermore, K_{IC} of the second layer of FGC 2 remained at 1.28 MPa m$^{-1/2}$, while K_{IC} of the first layer of FGC 2 (i.e. the SHA layer) decreased to 1.05 MPa m$^{-1/2}$. For the first sub-layer of FGC 3 (i.e. the TiO_2 layer), microcracks could not be induced under the indentation load of 2 kgf. Therefore, it could be inferred that fracture toughness of TiO_2 in the FGC was far higher than that of SHA coating. K_{IC} of the second sub-layer of FGC 3 which contained 50 wt % of TiO_2 was 1.76 MPa m$^{-1/2}$, which was still much higher than 0.47 MPa m$^{-1/2}$ that was obtained from the third sub-layer of FGC 3 (i.e. the SHA layer). These results indicated that both α-TCP and TiO_2 were effective in increasing microhardness and fracture toughness of pure hydroxyapatite coatings, with TiO_2 offering a greater toughening efficiency.

The current investigation has demonstrated that the addition of tougher ceramics (either α-TCP or TiO_2) can improve the fracture toughness of pure HA coatings significantly. Therefore, methods such as post-spray treatment [17] or introducing a toughening phase should be considered for enhancing the performance of HA coatings.

4. Conclusions

Dense HA coatings and bioactive FGCs can be produced by using flame spheroidized HA powders, spherical α-TCP powder and TiO_2 powder. Microhardness and fracture toughness of coatings are affected by characteristics of feedstock powders. The average microhardness value of SHA coatings decreases as the indentation load increases. The relationship between indentation load and indent diagonal length observed Meyer's law, with the Meyer parameter being lower than 2. The propagation of induced microcracks demonstrates anisotropy of the coatings, which is related to the lamellar structure produced by the plasma spray technique. Fracture toughness of SHA coatings decreases as the feedstock particle size increases. Methods such as introducing a toughening phase need to be used to improve the fracture toughness of HA coatings.

Acknowledgment

X. Y. Yang and Y. Wang are grateful to Nanyang Technological University for providing research studentships. Ms M.Y. Yong is thanked for providing technical assistance.

References

1. S. R. RADIN and P. DUCHEYNE, *J. Mater. Sci.: Mat. Med.* **3** (1992) 33.
2. J. H. C. LIN, M. L. LIU and C. P. JU, *ibid.* **5** (1994) 279.
3. P. FRAYSSINET, F. TOURENNE, N. ROUQUET, P. CONTE, C. DELGA and G. BONEL, *ibid.* **5** (1994) 11.
4. J. L. ONG, G. N. RAIKAR and T. M. SMOOT, *Biomaterials* **18** (1997) 1271.
5. A. SALOMONI, A. TUCCI, L. ESPOSITO and I. STAMENKOVIC, *J. Mater. Sci.: Mat. Med.* **5** (1994) 651.
6. E. CHAMPION, S. GAUTIER and D. B. ASSOLLANT, *ibid.* **7** (1996) 125.
7. V. V. SILVA and R. Z. DOMINGUES, *ibid.* **8** (1997) 907.
8. A. SLOSARCZYK and J. BIALOSKORSKI, *ibid.* **9** (1998) 103.
9. K. KURASHINA, H. KURITA, M. HIRANO, J. M. A. DE BLIECK, C. P. A. T. KLEIN and K. DE GROOT, *ibid.* **6** (1995) 340.
10. K. A. KHOR, P. CHEANG and Y. WANG, *J. Minerals, Metals Mater. Soc.* **49** (1997) 51.
11. P. LUO and T. G. NIEH, *Mater. Sci. Engng.* **C3** (1995) 75.
12. P. CHEANG and K. A. KHOR, *J. Mater. Process. Technol.* **48** (1995) 429.
13. F. KICK, ''Das Gesetz der proportionalen Widerstande und seine Anwendung'' (Edition Felix, Leipzig, 1985).
14. S. J. BULL, T. F. PAGE and E. H. YOFFE, *Phil. Mag. Lett.* **59** (1989) 281.
15. G. K. BESHISH, C. W. FLOREY, F. J. WORZALA and W. J. LENLING, *J. Thermal Spray Technol.* **2** (1993) 35.
16. J. B. PARK, ''Biomaterials science and engineering'' (Plenum Press, New York, 1984).
17. P. CHEANG, K. A. KHOR, L. L. TEOH and S. C. TAM, *Biomaterials* **17** (1996) 1901.

Received 19 June
and accepted 20 July 1998